THE ASTROPHYSICAL JOURNAL, 424:208–221, 1994 March 20

THE MAGNETIC FIELD IN THE OPHIUCHUS DARK CLOUD COMPLEX

ALYSSA A. GOODMAN[1]
Astronomy Department, University of California, Berkeley; and Astronomy Department, Harvard University, 60 Garden Street, Cambridge, MA 02138

AND

CARL HEILES
Astronomy Department, University of California, Berkeley, CA 94720
Received 1993 June 21; accepted 1993 September 22

ABSTRACT

By searching for the Zeeman effect in 21 cm H I spectra taken at 52 positions across the face of the Ophiuchus dark cloud complex, we have mapped out the strength of the line-of-sight magnetic field in the atomic gas associated with the complex.

The H I line profiles are comprised of multiple components, which are identified as arising from different physical regimes along the line of sight. A technique known as "Gaussianizing" is used to fit an independent field strength to each velocity component in each spectrum. The components with LSR velocities closest to the molecular gas in Ophiuchus are typically seen in self-absorption, as is to be expected if the H I giving rise to this component is indeed associated with relatively cold (i.e., molecular) gas. Thus, we take the field in the self-absorption component of the H I to be most representative of the dark cloud complex.

Using the line-of-sight field strengths measured via detection of the Zeeman effect in the H I self-absorption component, and optical polarization data which describe the plane-of-the-sky field structure, we present a model for the three-dimensional structure of the magnetic field near L1688. We estimate the mean uniform field for this region to be 10.2 μG, with an inclination to the line-of-sight of 32°. If there are four correlation lengths of the field along the line of sight, and the fluctuating component of the field is isotropic in three dimensions, then the typical strength of the nonuniform field is ~ 6 μG, and the ratio of energy in the nonuniform and uniform field is of order unity.

By comparing the line widths and Alfvén speeds for the positions where the Zeeman effect is detected in a self-absorption component, we find rough equality between kinetic and magnetic energy if the gas density in the region producing the H I self-absorption averages ~ 40 cm^{-3}.

Subject headings: ISM: individual (Ophiuchus Cloud) — ISM: magnetic fields — radio lines: ISM

1. INTRODUCTION

In this paper we seek to measure the strength of the magnetic field, $\boldsymbol{B}$, in the Ophiuchus dark cloud complex, and to measure its variation on scales of parsecs.

Optical (Vrba, Strom, & Strom 1976; Goodman et al. 1990), infrared (Wilking et al. 1979; Sato et al. 1988), and millimeter-wavelength (Tamura et al. 1993) polarimetry in Ophiuchus give the direction of $\boldsymbol{B}$ projected onto the plane of the sky. The polarimetric results show a highly ordered magnetic field throughout the complex, and the influence of magnetic fields in Ophiuchus has been proposed to explain everything from the large-scale orientation of dark cloud filaments (Vrba et al. 1976; Loren 1989a) to the orientation of jets, outflows, and elongated condensations associated with the young stars forming in the dark clouds (Loren, Wooten, & Wilking 1990; Mundy, Wooten, & Wilking 1990; Sato et al. 1988; Tamura et al. 1993; Tamura et al. 1990). By measuring the *strength of the magnetic field along the line of sight*, via detection of the Zeeman effect in H I spectral lines, we can add a third dimension, and a scale, to the description of the magnetic field in Ophiuchus.

The dark cloud complex in Ophiuchus is likely the remnant of a much larger molecular cloud which formed the stars we see today as the Scorpio-Centaurus OB association (Blaauw 1964; de Geus & Burton 1991). In its current state the complex is still a site of active star formation, consisting of several filamentary clouds extending out from two dense blobs, known as L1688 (a.k.a. the "ρ-Oph" cloud) and L1689.[2] The dense gas we call the dark cloud complex lies on the near side of an expanding bubble of gas created by stellar winds and supernova explosions. The interaction of the shell and the aboriginal molecular cloud produced the filaments (a.k.a. "streamers") seen today (de Geus 1992; see § 3.1).

The Ophiuchus complex is spectacularly evident on optical photographs (e.g., Ross & Calvert 1934; Myers & Ho 1975; Vrba et al. 1976) and has been extensively mapped in molecular spectral lines (Loren 1989a, b; de Geus & Burton 1991; Nozawa et al. 1991), with special attention paid to the L1688 region (e.g., Myers et al. 1978). Loren (1989a, b) mapped the complex in ^{13}CO, a tracer which shows an excellent correlation with visual extinction and can provide fine velocity and spatial resolution. Loren identified 89 "clumps" in the ^{13}CO maps and tabulated their properties, providing an especially complete database for studying the physics of dark star-forming clouds. Several infrared and submillimeter continuum studies have revealed scores of young and forming stars

[1] Alfred P. Sloan Fellow.

[2] Figure 6 can be used as a finding chart for the various Lynds clouds (e.g., L1688) in the Ophiuchus dark cloud complex.

embedded primarily in the clumps associated with L1688 and L1689 (see Wilking 1990 and Evans & Lada 1991 and references therein).

In this paper, we concern ourselves primarily with the atomic gas associated with the dark clouds in Ophiuchus, and the magnetic field in that gas. In § 2 we describe the method used to derive field strengths from H I spectral line observations, which amounts to measurement of the Zeeman effect in spectral lines comprised of multiple velocity components. In § 3 we explain the spatial and kinematic distribution of H I along the line of sight to Ophiuchus, and we discuss the atomic gas associated with the molecular clouds (often seen in self-absorption) in some detail. We present a model for the three-dimensional structure of the magnetic field near L1688 in § 3.4. We conclude that the field strengths measured in the self-absorption-producing atomic gas imply rough equality between kinetic and magnetic energy if the gas density in the region producing the self-absorption averages ~ 40 cm^{-3}.

2. DATA

2.1. H I *Zeeman Observations*

The new magnetic field measurements presented in this paper come from observations of the Zeeman effect in the 21 cm line of H I. All of the data were obtained using the 85 ft (26 m) telescope at Hat Creek,[3] with a system similar to the one described in Heiles (1988) and Heiles & Stevens (1986). The full width at half-power of the Hat Creek dish at 21 cm is approximately 36′. As in previous observations (e.g., Heiles 1988), the 1024 channel autocorrelator was split into two independent 512 channel banks, each simultaneously observing opposite circular polarization. In observing Ophiuchus, we used a bandwidth of 312.5 kHz, giving a channel separation of 610 Hz, equivalent to 0.129 km s^{-1} at 1420 MHz.[4] Thus, the velocity resolution after the spectra have been Hanning-smoothed is 0.26 km s^{-1}. Each position was observed for approximately 10 hours, giving an rms noise level of ~ 0.02 K, with a system temperature of 45 K.

The Zeeman splitting of the 21 cm H I line corresponds to 2.8 Hz/μG. So, fields typical of those measured in dark clouds (~ 10 μG) will produce splittings corresponding to only a small fraction of a channel ($\sim 5\%$) in the setup described above. Therefore, as is typical in Zeeman observations of thermally excited radio spectral lines, we cannot resolve individual components of the Zeeman pattern. Instead, we exploit the fact that the positively and negatively shifted components of the pattern have opposite sense of circular polarization. We construct the Stokes V-spectrum (RCP-LCP) and search for patterns proportional to the derivative of the line profile, indicative of the Zeeman effect (cf. Heiles & Stevens 1986; Goodman 1989; Crutcher et al. 1993). (Note that by "line profile" we refer to (RCP + LCP)/2, or half the Stokes I.)

2.2. "*Gaussianizing*"

In cases where many velocity components are present at a single position, the Zeeman pattern in the observed V-spectrum can be very difficult to interpret. It is possible for a different field strength to be associated with each component, so that the observed V-spectrum becomes the superposition of several difficult-to-disentangle Zeeman patterns. In this paper we have used a technique Heiles has used previously, which we call "Gaussianizing" (see § III of Heiles 1988).

Gaussianizing consists of modeling an observed line profile to be the sum of $N_{\rm Gauss}$ Gaussians, each of which can have any value of $B_\parallel$ associated with it, where $B_\parallel$ is the line-of-sight field strength. The model Zeeman pattern for each Gaussian is proportional to the product of the Zeeman splitting factor (2.8 Hz/μG for H I at 1420 MHz), the derivative of the Gaussian, and $B_\parallel$.[5] So, once a specific Gaussian-sum model for the line profile is arrived at, the observed V-spectrum can be modeled as the sum of the Zeeman patterns for the individual components, with the field strengths for the $N_{\rm Gauss}$ components being the only free parameters.

The Gaussianizing technique is best illustrated by example. In Figure 1 we show how the model is applied to a position in Ophiuchus (position no. 11 in Table 1). Figure 1*a* illustrates how the line profile is broken down into four Gaussian components (labeled A, B, C, and D), one of which (B) has negative amplitude and represents self-absorption. Figure 1*b* shows the observed and modeled Stokes $I/2$- and V-spectra, and it is clear that there is a good fit. Two of the components (A and D) do not give significant detections of $B_\parallel$, and two (B and C) do (see Table 1). Components B and C both give $B_\parallel \approx 9.7$ μG, at better than about the 5 σ level, and they both have narrow line widths and similar LSR velocities. Encouragingly, their LSR velocities are also similar to that of the molecular gas in the region (see § 3.1).

The Gaussianizing technique is not infallible. In most cases one can ultimately see physical justification for the choice of components, but there are still many cases where the breakdown of the line profile is somewhat arbitrary. It is reassuring, however, that in cases where it is not clear what value of $N_{\rm Gauss}$ to use, components which give significant detections of $B_\parallel$ usually persist across several beam widths.

3. RESULTS

3.1. *Kinematic Breakdown of the* H I *in the Direction of the Ophiuchus Complex*

The dynamics of the gas and stars in Scorpius Centaurus have been analyzed in detail by de Geus and his collaborators (de Geus 1988, 1992; de Geus, Bronfman, & Thaddeus 1990; de Geus & Burton 1991; de Geus, de Zeeuw, & Lub 1989) and by Cappa de Nicolau & Pöppel (1986). In this paper we will adopt de Geus's model of the Upper Scorpius region, where the Ophiuchus dark cloud complex lies on the near side of an expanding bubble of gas created by stellar winds and supernova explosions in an association of early-type stars in Upper Scorpius (part of the Sco OB2 association). Using both photometric and proper motion studies of stars in the direction of the Ophiuchus complex, de Geus et al. (1989) estimate that the dark cloud complex lies at 125 ± 25 pc from the Sun, with an extent of about 45 ± 25 pc along the line of sight. (This distance disagrees with the estimate of 160 pc made by Bertiau 1958, which is used in Loren 1989a, b and several other studies.)

In de Geus's (1992) picture, it is assumed that the region of

[3] This work presents some of the last data ever taken with the 85-foot, which was destroyed by a wind gust on 1993 January 21. We dedicate this paper to the memory of this fine instrument.

[4] The majority of the data were taken in 1991 and 1992 and use this correlator setup. The remaining (older) data has velocity resolution twice as coarse.

[5] See Crutcher et al. (1993) or Goodman (1989) for a detailed description of why this type of Zeeman observation is only sensitive to the line-of-sight component of the field.

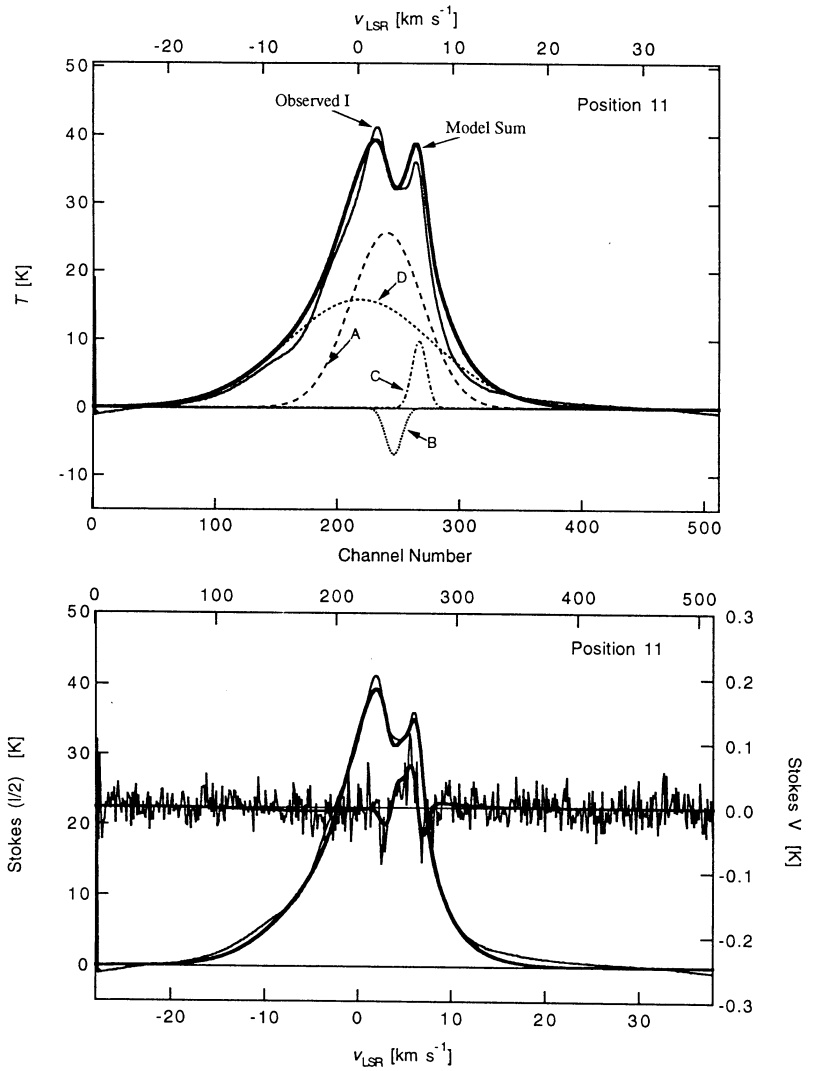

FIG. 1.—Model and data illustrating the Gaussianizing technique as applied to a position in Ophiuchus ("Position no. 11": $\alpha_{1950} = 16^h21^m5$, $\delta_{1950} = -25°18'$). (*a*) Decomposition of the line profile into four Gaussian components (labeled A, B, C, and D). (*b*) Observed and modeled Stokes $I/2$- and V-spectra, using the model shown in (*a*). Two of the components (A and D) do not give significant detections of $B_{\|}$, and two (B and C) do, with $B_{\|} \approx 9.7$ μG for each, at better than about the 5 σ level.

interest in Upper Scorpius was originally filled with gas at LSR velocity comparable to the molecular gas we see today. The molecular cloud was larger than what we see today, and the L1688–L1689 region (see Fig. 6) was a dense clump in the cloud. An association of several early-type stars "behind" the Ophiuchus dark clouds produce winds and supernovae which create an expanding bubble, with expansion velocity 10–15 km s^{-1}, depending on the local density of the ambient medium. Much of the interior of the shell is ionized by the early-type stars, and there is a contact discontinuity at the inside surface of the shell. The interaction of the shell with the ambient gas produces a shock front at the outside edge of the shell, and the shell layer itself is filled with "swept-up" material. There is a -12 km s^{-1} feature seen in H I emission in the region that does not overlap with the dark clouds (Sancisi & van Woerden 1970), and that represents the part of the shell which has passed through the lowest density ambient material and has not been slowed down significantly. The encounter of the expanding shell with the densest gas (L1688-L1689) in Ophiuchus punched a hole in the shell, creating the relatively low abundance of H I seen in the direction of the dark cloud complex today. De Geus (1992) further suggests that this encounter may have also triggered the star formation we see in L1688 and L1689 today. In addition, the passage of the shock caused molecular gas to be swept off the dense core, which was then deposited as elongated clouds "to the side of the region avoided by the shell," creating the filamentary clouds (streamers) we see today.

In order to model the distribution of H I along the line of sight through the Ophiuchus dark cloud complex, we applied the Gaussianizing technique (see § 2.2) to all the positions where we measured the Zeeman effect, shown in Figure 2. We aspired to identify components in the spectra that could be placed into the context of a physical picture like the one above. We limited N_{Gauss} to be no greater than 4, and Table 1 shows all components fit at each position.

In general, the components we identified can be broken down into three categories: wide emission, narrow emission

TABLE 1

SUMMARY OF H I ZEEMAN OBSERVATIONS IN OPHIUCHUS

Position (1)	R.A. (1950) (hours) (2)	Decl. (1950) (degrees) (3)	V_{LSR} (km s^{-1}) (4)	T_A (K) (5)	ΔV (km s^{-1}) (6)	$B_{\parallel}$ (μG) (7)	$\sigma_{B_{\parallel}}$ (μG) (8)	^{13}CO Clump (9)	^{13}CO V_{LSR} (km s^{-1}) (10)	^{13}CO ΔV (km s^{-1}) (11)	^{13}CO Mass ($M_\odot$) (12)	Percent of H I Beam in ^{13}CO Clump (13)
1.....	16.27	−23.47	0.4	52.0	7.0	**4.0**	**0.8**	R4	4.3	0.7	11	50%
			0.6	0.7	0.8	−42.8	19.6					
			4.2	−6.6	1.9	10.6	3.7					
			4.9	20.6	3.9	−1.2	1.8					
2.....	16.28	−23.92	−11.0	8.6	8.7	3.2	4.1	N/A	N/A	N/A	N/A	N/A
			2.3	68.6	9.5	0.9	0.6					
			3.7	−24.9	3.5	**4.1**	**1.0**					
			8.1	−11.3	3.8	5.8	2.2					
3.....	16.29	−23.05	−10.9	5.6	7.4	8.7	6.0	N/A	N/A	N/A	N/A	N/A
			0.7	50.5	9.4	1.7	0.8					
			4.9	5.5	1.7	4.4	2.8					
4.....	16.31	−24.17	−9.8	6.6	9.4	−31.7	15.5	R6/8	4.8	0.9	3	5
			0.2	11.4	1.4	4.4	1.7					
			1.4	62.7	9.4	−1.0	1.1					
			2.9	−23.2	3.5	**12.1**	**1.5**					
5.....	16.31	−23.61	0.1	51.7	7.6	**−4.2**	**0.9**	R7	2.9	0.7	29	70
			0.4	12.3	1.9	4.7	1.9					
			3.9	−5.3	1.3	**14.5**	**3.4**					
			5.4	17.9	3.8	−0.2	1.8					
6.....	16.32	−24.50	−8.9	6.0	9.3	−5.4	14.3	R9	3.3	0.5	3	5
			1.7	69.9	9.2	−2.5	1.0					
			1.9	−20.7	2.0	**11.8**	**1.2**					
			3.9	−27.2	2.5	**10.7**	**1.0**					
7.....	16.33	−23.25	−9.7	5.1	8.6	24.2	14.7	R11	3.6	0.5	3	5
			1.0	55.0	9.4	1.1	0.9					
			2.8	−16.1	2.9	**6.8**	**1.3**					
			5.1	2.7	1.0	6.7	4.2					
8.....	16.34	−22.83	0.8	58.9	8.7	−0.3	0.8	R12	3.2	0.5	19	25
			2.5	−14.3	2.5	**9.3**	**2.0**					
			4.9	8.7	1.5	−2.0	2.4					
9.....	16.35	−24.20	−0.8	49.8	6.4	−1.2	1.0	R14	1.7	0.6	18	10
			0.0	16.0	2.0	5.4	1.6					
			4.1	−10.8	1.5	**9.1**	**2.1**					
			5.2	35.5	4.3	−2.1	1.1					
10.....	16.35	−23.94	−1.0	52.5	6.6	−0.6	0.7	R16	2.4	0.9	9	10
			0.1	19.3	1.9	3.4	1.0					
			3.9	−10.5	1.3	**8.0**	**1.5**					
			5.0	36.1	4.4	−0.3	0.9					
11.....	16.36	−25.30	0.1	15.8	15.5	−6.2	3.5	R20	3.7	0.8	1	5
			3.0	25.7	7.6	−1.5	1.4					
			3.7	−6.9	1.8	**9.4**	**2.1**					
			6.4	9.8	1.6	**9.9**	**1.3**					
12.....	16.36	−23.50	−10.6	3.0	6.4	32.6	19.2	R19	2.1	0.8	6	20
			0.8	60.3	9.9	−0.5	0.8					
			2.3	−18.2	2.2	**5.3**	**1.2**					
			3.8	−11.7	1.3	**6.1**	**1.4**					
13.....	16.36	−24.68	−0.7	37.0	6.5	1.0	1.5	R17	3.0	1.1	23	50
			0.9	11.8	2.7	−0.1	3.0					
			4.5	−11.4	1.6	7.7	2.4					
			5.2	34.6	4.2	−0.5	1.4					
14.....	16.39	−24.27	−1.9	29.8	3.9	**4.3**	**0.9**	R22	*3.2*	1.7	844	95
			1.1	38.6	3.1	2.3	0.7					
			4.6	−14.6	1.5	**5.0**	**1.3**					
			5.0	38.3	3.5	−2.4	0.9					
15.....	16.40	−24.45	−1.9	25.4	4.0	**3.2**	**0.9**	R22	*3.2*	1.7	844	70
			1.4	35.5	3.2	2.2	0.7					
			4.9	−9.6	1.5	**13.2**	**1.7**					
			5.2	36.8	3.7	**3.9**	**0.8**					
16.....	16.41	−24.78	−2.2	14.9	4.1	3.0	1.5	R25	*3.5*	1.3	368	40
			1.1	13.4	2.8	**6.2**	**1.2**					
			3.9	27.8	6.8	−2.0	1.0					
			6.2	9.7	1.9	**10.2**	**1.3**					
17.....	16.41	−24.58	−1.7	22.1	4.9	3.5	1.9	R25	*3.5*	1.3	368	60
			1.3	16.2	2.7	4.3	1.7					
			4.3	27.2	5.8	−0.7	1.7					
			6.2	9.5	1.7	**14.1**	**2.3**					
18.....	16.41	−24.18	−1.9	26.6	4.3	1.2	0.9	R26	*3.3*	1.4	206	60
			1.2	31.6	2.9	−0.4	0.7					
			4.5	−9.3	1.4	6.1	1.8					
			4.8	31.7	3.5	−2.5	0.9					

TABLE 1—*Continued*

Position (1)	R.A. (1950) (hours) (2)	Decl. (1950) (degrees) (3)	V_{LSR} (km s^{-1}) (4)	T_A (K) (5)	ΔV (km s^{-1}) (6)	$B_{\|\|}$ (μG) (7)	$\sigma_{B_{\|\|}}$ (μG) (8)	^{13}CO Clump (9)	^{13}CO V_{LSR} (km s^{-1}) (10)	^{13}CO ΔV (km s^{-1}) (11)	^{13}CO Mass ($M_\odot$) (12)	Percent of H I Beam in ^{13}CO Clump (13)
19.....	16.42	−24.06	−1.5	22.4	5.0	**3.8**	**0.6**	R26	*3.3*	1.4	206	85
			1.4	23.2	2.9	**2.1**	**0.5**					
			4.5	−6.5	1.3	3.9	1.2					
			4.9	27.4	3.4	1.3	0.5					
20.....	16.42	−23.83	−1.3	27.0	5.4	**4.9**	**0.8**	R29	3.0	0.8	12	15
			1.2	20.3	2.6	**3.2**	**0.7**					
			4.4	−9.9	1.3	**6.1**	**1.2**					
			4.7	29.7	3.2	1.0	0.7					
21.....	16.44	−24.58	1.7	31.2	10.6	3.8	2.1	R25	*3.5*	1.2	368	60
			1.7	9.2	1.8	5.0	2.9					
			4.9	11.6	2.0	8.3	3.0					
			5.5	26.7	3.5	**8.9**	**1.8**					
22.....	16.44	−24.14	1.1	38.8	10.4	2.0	1.0	R26	*3.3*	1.4	206	70
			1.4	7.5	1.9	3.8	2.1					
			4.5	−4.9	1.1	2.0	2.5					
			5.4	16.0	2.6	2.8	1.2					
23.....	16.45	−24.83	1.6	29.2	10.8	1.7	1.6	N/A	N/A	N/A	N/A	N/A
			1.8	16.0	2.2	**6.2**	**1.4**					
			5.1	−14.2	2.1	−2.0	2.0					
			5.4	39.4	3.8	1.5	1.0					
24.....	16.46	−24.31	−1.2	19.5	7.9	−4.1	2.8	N/A	N/A	N/A	N/A	N/A
			3.9	−14.3	2.3	9.2	2.8					
			4.2	43.4	5.8	0.2	1.4					
			6.0	4.2	1.4	−1.2	6.2					
25.....	16.47	−24.74	−0.3	15.7	6.9	**8.0**	**1.3**	R53	4.5	1.3	61	35
			2.0	15.6	2.5	**8.2**	**0.8**					
			5.0	28.7	4.6	**3.9**	**0.6**					
			6.4	7.6	1.7	1.4	1.3					
26.....	16.49	−23.77	0.2	22.9	9.1	2.2	1.2	R37	*2.5*	1.0	133	60
			1.4	7.9	2.6	0.1	1.9					
			5.0	16.3	4.7	**−4.7**	**1.3**					
			5.5	9.3	1.6	4.5	1.3					
27.....	16.49	−24.95	0.8	20.4	10.4	2.6	3.5	R55	*4.4*	1.6	83	70
			2.2	9.9	2.3	9.7	3.3					
			4.5	27.0	5.3	2.1	1.8					
			6.3	9.0	1.8	−4.1	3.1					
28.....	16.49	−24.43	0.8	20.6	11.1	5.2	3.4	R57	*3.9*	1.4	202	95
			1.8	6.6	1.9	−1.4	3.8					
			3.6	23.0	5.8	−2.4	2.1					
			5.7	10.9	2.0	−4.0	2.3					
29.....	16.50	−24.23	0.7	25.8	11.5	7.1	2.6	R61	3.4	0.5	11	30
			1.8	8.1	2.2	1.6	3.1					
			4.2	15.4	5.5	1.0	2.8					
			5.6	12.6	2.0	−5.4	2.0					
30.....	16.50	−24.72	1.4	20.2	10.2	**7.7**	**1.3**	R60	3.8	0.7	31	20
			2.1	16.8	2.7	2.6	0.8					
			5.1	20.5	3.7	−1.0	0.8					
			6.2	5.1	1.4	3.6	1.8					
31.....	16.50	−24.04	−1.1	18.7	7.9	4.6	3.2	N/A	N/A	N/A	N/A	N/A
			3.8	−10.2	2.1	−3.1	3.7					
			4.0	40.9	6.0	−0.9	1.5					
			6.0	8.1	1.4	5.4	3.4					
32.....	16.52	−24.53	1.1	22.7	10.7	2.8	3.4	R65	3.8	0.6	39	35
			1.8	2.3	1.6	−9.8	10.9					
			3.3	24.7	5.4	−2.5	2.2					
			5.6	11.2	1.9	−5.5	2.3					
33.....	16.53	−23.42	0.2	4.9	26.3	−0.2	9.2	R42	2.6	0.5	8	35
			0.7	17.9	12.6	2.8	1.9					
			1.6	13.4	3.2	0.7	1.0					
			5.4	21.2	3.8	−1.6	0.7					
34.....	16.53	−24.69	1.5	20.0	11.0	**17.2**	**1.9**	R65	3.8	0.6	39	40
			2.7	21.9	4.2	−2.6	1.0					
			5.6	15.5	2.7	**−6.2**	**1.2**					
			5.9	1.8	1.2	11.5	6.7					
35.....	16.55	−23.88	−1.5	17.5	7.6	1.1	3.0	N/A	N/A	N/A	N/A	N/A
			3.6	−2.1	1.1	−0.6	9.5					
			3.8	36.4	6.2	0.9	1.3					
			5.6	5.1	1.4	12.8	4.3					
36.....	16.55	−21.99	1.6	40.4	7.9	2.7	1.0	R81	1.7	0.8	32	90
			2.1	−7.7	2.1	9.5	2.8					
			4.4	6.7	1.3	3.5	2.3					

TABLE 1—*Continued*

Position (1)	R.A. (1950) (hours) (2)	Decl. (1950) (degrees) (3)	V_{LSR} (km s^{-1}) (4)	T_A (K) (5)	ΔV (km s^{-1}) (6)	$B_{\|\|}$ (μG) (7)	$\sigma_{B_{\|\|}}$ (μG) (8)	^{13}CO Clump (9)	^{13}CO V_{LSR} (km s^{-1}) (10)	^{13}CO ΔV (km s^{-1}) (11)	^{13}CO Mass ($M_\odot$) (12)	Percent of H I Beam in ^{13}CO Clump (13)
37.....	16.56	−24.23	−1.7	19.2	6.4	−1.3	1.9	R68/69	4.2	0.5	36	50
			3.5	43.8	6.1	1.1	0.8					
			3.7	−3.3	1.1	−7.1	4.6					
			5.8	7.7	1.3	**−8.4**	**2.0**					
38.....	16.56	−23.46	−1.6	15.9	6.8	5.3	3.1	R48	1.9	0.7	7	15
			1.4	7.6	2.2	−4.6	3.4					
			4.7	34.8	5.9	3.5	1.3					
39.....	16.59	−24.20	2.4	38.7	7.6	3.3	1.2	R71	4.1	0.6	19	25
			3.9	−0.6	0.6	−19.6	22.0					
			5.8	10.8	1.7	−3.0	2.1					
40.....	16.59	−22.19	1.9	39.9	9.0	0.4	1.1	N/A	N/A	N/A	N/A	N/A
			2.5	−4.4	1.6	7.1	4.2					
			4.9	6.8	1.5	7.7	2.6					
41.....	16.61	−22.78	−2.3	11.6	5.6	**9.5**	**2.5**	N/A	N/A	N/A	N/A	N/A
			3.6	−11.2	2.1	0.4	1.5					
			3.9	50.2	7.0	−1.9	0.7					
42.....	16.61	−21.58	−1.3	−8.9	3.2	3.5	2.3	N/A	N/A	N/A	N/A	N/A
			0.3	2.7	1.3	14.4	4.7					
			1.0	39.4	8.9	−0.7	0.9					
			4.2	10.6	1.8	−0.2	1.4					
43.....	16.62	−24.08	2.7	47.5	7.4	**3.0**	**0.8**	R74	4.6	1.2	44	45
			3.7	−3.8	1.3	−6.3	4.2					
			5.9	10.4	1.6	−3.9	1.7					
44.....	16.63	−22.23	−3.2	14.9	4.5	−3.4	2.9	R83	2.0	1.0	40	65
			1.3	36.6	4.2	0.6	1.3					
			4.8	30.9	3.0	−2.6	1.1					
			7.3	14.2	4.2	−5.0	2.7					
45.....	16.65	−23.98	3.1	48.6	7.5	**3.0**	**0.6**	R75	4.9	1.2	101	80
			3.7	−7.8	2.0	−3.4	2.0					
			6.2	6.1	1.3	−0.1	1.9					
46.....	16.65	−21.17	−4.1	12.9	4.6	7.9	2.5	N/A	N/A	N/A	N/A	N/A
			2.2	49.0	6.1	2.4	0.9					
			2.4	−14.7	2.3	**6.6**	**1.6**					
47.....	16.68	−21.70	0.8	16.3	4.6	−0.6	3.4	R86	2.3	1.0	52	75
			2.2	34.1	16.7	−4.8	3.5					
			4.8	14.7	2.1	−3.6	2.4					
			11.0	−1.4	1.9	16.4	23.0					
48.....	16.70	−24.54	3.7	28.5	7.4	−0.1	0.8	N/A	N/A	N/A	N/A	N/A
			7.0	10.2	2.9	0.5	1.6					
			9.6	8.0	2.0	−3.6	1.7					
49.....	16.70	−23.94	0.2	19.0	4.2	0.3	1.0	R76	4.8	0.5	6	10
			2.3	7.0	2.1	−0.8	1.7					
			5.0	30.1	5.6	**−4.4**	**0.8**					
50.....	16.70	−23.34	−1.1	16.6	4.7	**6.7**	**0.8**	**N/A**	**N/A**	**N/A**	**N/A**	**N/A**
			2.1	19.6	3.1	−0.8	0.6					
			3.7	11.8	20.5	−3.0	2.2					
			5.0	24.2	3.6	−0.5	0.5					
51.....	16.71	−21.32	−5.4	12.6	4.5	−7.7	3.2	R87	2.5	1.3	51	85
			0.5	45.2	5.6	−0.1	1.0					
			4.2	17.8	2.4	−1.1	1.2					
			6.8	14.7	5.7	−4.2	2.6					
52.....	16.72	−23.80	1.8	37.2	7.0	−4.8	1.6	R76	4.8	0.5	6	15
			4.2	−1.5	1.0	9.1	14.7					
			6.3	18.0	4.2	−9.1	2.7					
			10.0	7.2	2.7	−3.5	5.3					

NOTES.—Col. (1) Position number; cols (2)–(3) equatorial coordinates, epoch 1950; col. (4) LSR velocity, col. (5) antenna temperature, and col. (6) FWHM line width of each Gaussian component of the observed H I line profile at this position number; col. (7) line-of-sight magnetic field strength and col. (8) its 1 σ error—boldface values in cols. (7) and (8) indicate "significant" field detections, where $B_{\|\|}/\sigma_{B_{\|\|}} \geq 3.5$; col. (9) ^{13}CO clump associated with this position number, from Loren 1989a; col. (10) LSR velocity of ^{13}CO emission (for clump in col. [9], according to Loren 1989a)—*italicized* entries indicate that the ^{13}CO emission is saturated, so the ^{13}CO V_{LSR} may be considered suspect in these cases; col. (11) FWHM line width of ^{13}CO emission, and col. (12) inferred mass for clump in col. (9), from Loren 1989a; col. (13) percentage of the H I beam area at the position in col. (1) associated with clump in col. (9).

(FWHM line width <4 km s^{-1}), and self-absorption. For the purposes of this paper, we will concentrate on the narrower features in the H I spectra with velocities similar to the molecular gas along the line of sight. We note for those interested, however, that line parameters and field strength determinations for *all* components are listed in Table 1.

We used the extensive ^{13}CO maps presented in Loren (1989a, b) to determine the approximate LSR velocity of the molecular gas at any given position in the Ophiuchus dark cloud complex. In Table 1, for each H I position observed, we list the name of the nearest ^{13}CO-identified clump (Loren 1989a), along with the velocity Loren assigns to it. Since the H I

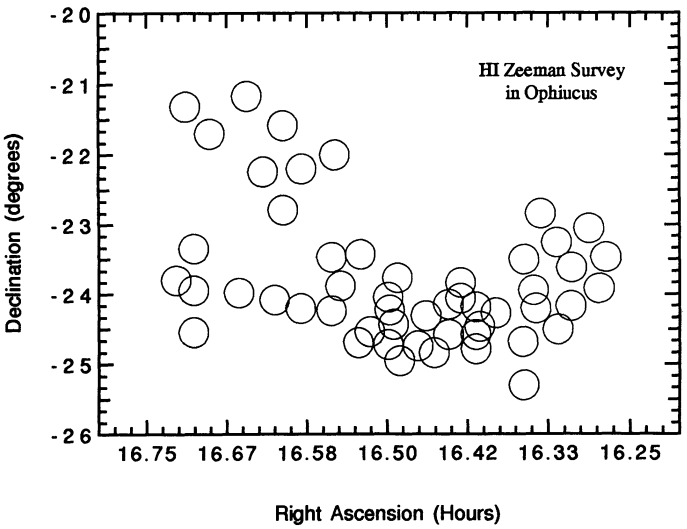

FIG. 2.—Summary of positions observed. The symbol size corresponds to the FWHM beam size at Hat Creek, approximately 36′. Note that the map is oversampled in some regions.

beam is so large compared to the size of many of Loren's clumps, we also list approximately what percentage of the beam area is associated with each clump.

In the region near L1688, the ^{12}CO and the ^{13}CO line profiles are highly non-Gaussian, and grossly asymmetric, covering a velocity range from about 2.5 to 5.5 km s^{-1} in ^{13}CO, and a still wider range in ^{12}CO (see spectra in Fig. 1 of Wilking & Lada 1983). Some of the asymmetry in the ^{12}CO and ^{13}CO lines is due to self-absorption on the high-velocity side of the lines. The C^{18}O line, which traces higher density gas, shows no self-absorption and is more symmetric, with FWHM width of almost 2 km s^{-1} (Wilking & Lada 1983). The position-velocity diagrams shown in Loren (1989b) imply similarly complex line profiles associated with many of the more massive condensations in the Ophiuchus complex. In fact, in listing the velocity of each of his clumps, Loren (1989a) identifies certain positions as suffering from saturation in the ^{13}CO line. In these cases, it is difficult to determine a truly characteristic molecular-gas velocity, so comparisons of H I and ^{13}CO velocity are not as useful as in lower density regions (^{13}CO LSR velocities for saturated positions are italicized in Table 1). Even in the positions where ^{13}CO is not saturated, when one takes into account all the velocity structure in the molecular gas itself, and the fact that Lorens clumps typically do not fill the H I beam, it can be complicated to quantify how "well" atomic (i.e., H I) velocities match molecular velocities.

In total, we observed 52 independent positions in Ophiuchus, and identified three or four independent Gaussian components per position, for a total of 196 components in our data set. Figure 3 shows line width as a function of antenna temperature for all 196 components, and shows the delineation of the three regimes we call "wide emission," "narrow emission," and "self-absorption."

The difference between the ^{13}CO LSR velocity (see Table 1) and the H I LSR velocity for each component is defined as

$$v_{\rm DIFF} = v_{\rm LSR}({\rm H\ I}) - v_{\rm LSR}(^{13}{\rm CO})\ . \qquad (1)$$

The distribution of $v_{\rm DIFF}$ is distinctly different for each of the three categories of line component, as illustrated in Figure 4. When H I is seen in self-absorption, its Gaussian-fit LSR velocity is within 1–2 km s^{-1} of the local ^{13}CO velocity assigned by Loren. In the narrow emission components, we see two peaks in the distribution of $v_{\rm DIFF}$, one that is blueshifted with respect to the CO by about -2 km s^{-1}, and one that is redshifted by approximately the same amount. The distribution of $v_{\rm DIFF}$ for the wide emission components is relatively symmetric, peaked at about -2.5 km s^{-1}, with a spread (FWHM) of about 3.5 km s^{-1}. We also detect the "-12 km s^{-1} wind" discovered by Sancisi & van Woerden (1970) as "wide emission" at four positions near the western end of our survey, but no significant Zeeman detections are associated with this component, so we will not discuss it in detail in this paper.

Figure 5 illustrates the spatial extent of the narrow emission, wide emission, and self-absorption components. As we might expect, the wide emission component is present at every position observed. Self-absorption is also widespread throughout the complex, and its strength does not appear to be correlated with molecular emission (see ^{13}CO contours in Fig. 5). The spatial distribution of self-absorption shown in Figure 5 is consistent with the 9′ resolution map of the H I self-absorption feature in the region near L1688 and L1689 made by Minn (1981). Minn notes the lack of spatial correlation between atomic and molecular gas in the region, and good agreement in LSR velocity between the H I self-absorption and molecular emission. The narrow emission is displayed in two maps, broken down by velocity. The gas that is producing narrow emission lines with $v_{\rm LSR}({\rm H\ I}) < v_{\rm LSR}(^{13}{\rm CO})$ appears to be more localized (near the L1688 and L1689 cores) than the gas with $v_{\rm LSR}({\rm H\ I}) > v_{\rm LSR}(^{13}{\rm CO})$, which is spread throughout much of the complex. Several positions show "narrow emission" at more than one velocity.

In accord with de Geus's picture, one can model each of the components as arising from a distinct regime. The self-absorption is produced when very cold H I gas associated with the molecular clouds is seen in front of warm H I associated

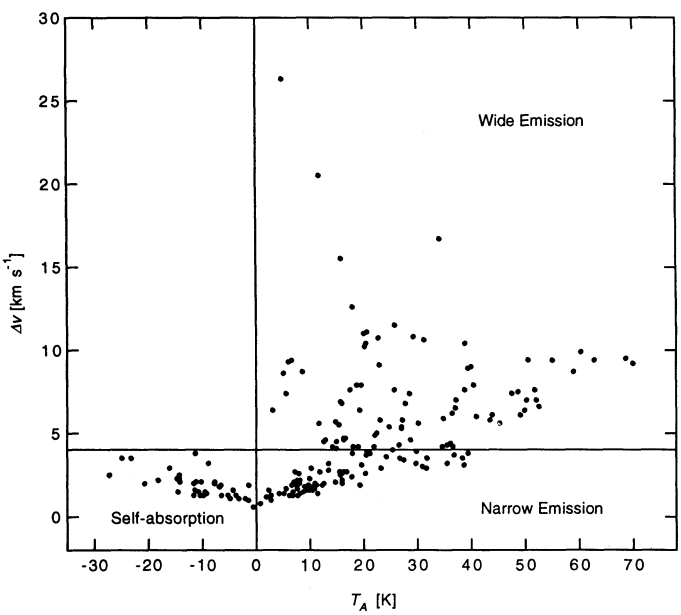

FIG. 3.—Line width as a function of antenna temperature, for all 196 components listed in Table 1. The cross-hair shows the division of the parameter space into the self-absorption, narrow emission, and wide emission components discussed in the text.

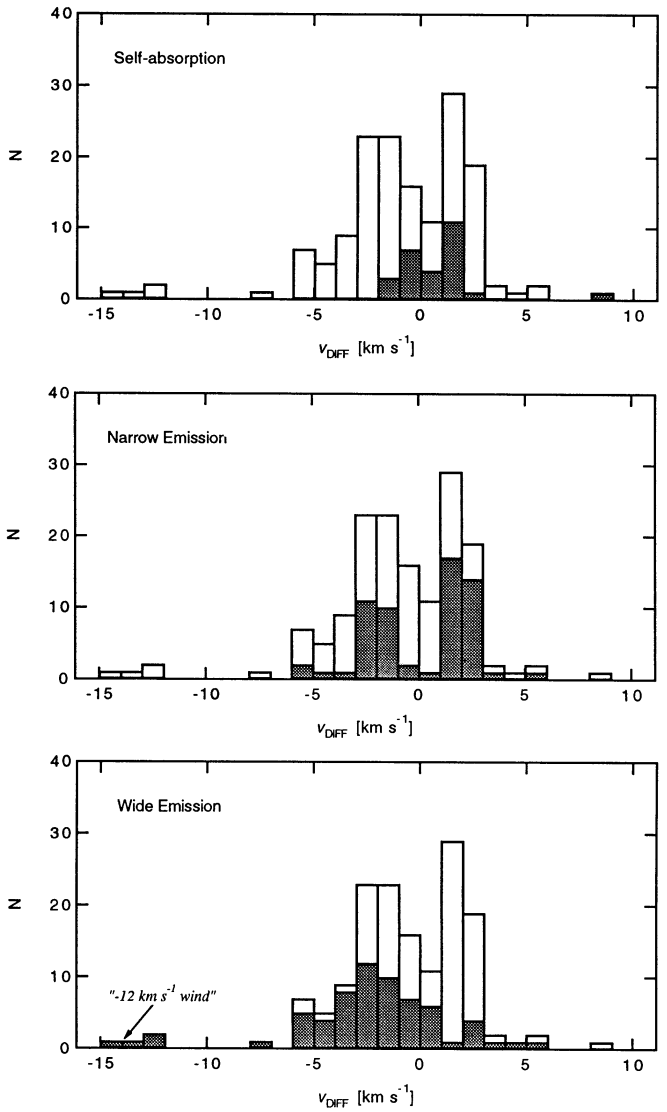

FIG. 4.—Distribution of $v_{DIFF} = v_{LSR}(\text{H I}) - v_{LSR}(^{13}\text{CO})$ for the self-absorption, narrow emission, and wide emission components of the spectra listed in Table 1. (See Fig. 3 and text for the definition of these three components.) The outlined distribution shown as a background in every panel represents the sum of the three distributions shown individually.

with the interior of the shell created by the stars behind the dark cloud complex. The narrow emission with velocities blueshifted with respect to the CO is on the near side of the (expanding) shell, and closer to us than most of the molecular gas, having swept past it. The wide emission, which is also almost all blueshifted with respect to the CO, is likely to also represent gas closer than the molecular clouds. The redshifted narrow emission is somewhere behind the molecular clouds in this scenario, although its velocity is not far from that of the CO, so it is not likely to be too far from the molecular gas.

Generally, we believe that the self-absorption and narrow emission components with velocities within ~ 2 km s^{-1} of the local ^{13}CO velocity originate in gas associated with the Ophiuchus molecular cloud complex, and we will concentrate our analysis of the magnetic field, comprising the remainder of this paper, almost exclusively on these components.

3.2. "*Significant*" *Detections*

In Table 1 we have highlighted all field measurements where the error in the fitted field, $\sigma_{B_\parallel}$, is equal to or less than $B_\parallel/3.5$. Experience has shown that detections at this level of significance are usually reliable. (See Troland & Heiles 1982 and Heiles 1988 for discussions of instrumental effects, such as beam squint, that can create patterns that mimic the Zeeman effect.)

The subsequent analysis in this paper is restricted to fields measured with $B_\parallel \geq 3.5\sigma_{B_\parallel}$. In total, for the 52 positions observed, we achieved 44 such "significant" detections. Note, however, that this statistic does not imply that the field was detected at 44 out of 52 positions: many detections are in multiple components at the same position and are counted individually.

3.3. *The Field in the Self-Absorption Component*

Figure 6 shows $B_\parallel$ at all of the positions where significant ($B_\parallel \geq 3.5\sigma_{B_\parallel}$) fields are detected in H I self-absorption. All but one of these detections are near the L1688 cloud, which contains the active star formation region associated with ρ-Ophiuchus (near 16^h24^m; $-24°26'$). The other significant detection of the Zeeman effect in self-absorption is associated with the filamentary dark cloud L1755. We caution that the spectra for the positions where we have "detected self-absorption" can also be fitted as the sum of Gaussians all with positive amplitude, by placing strong narrow features on either side of the alleged "self-absorption" dip in the spectrum. We choose to use the models which include a true self-absorption (negative amplitude) component because the average velocity of the self-absorption we find matches the velocity of the molecular gas better than any emission components in models which contain no self-absorption.

The abundance of Zeeman detections in the L1688 region provides us with the opportunity to study the structure of the line-of-sight magnetic field there. The H I responsible for the absorption is presumably associated with the molecular cloud, since the typical difference between the H I and the peak ^{13}CO velocity near L1688 is relatively small, with v_{DIFF} on the order of 1 km s^{-1} (see § 3.1). Thus, we expect that the fields measured in the self-absorption component are also likely to be associated with the dark (i.e., molecular) cloud.

3.4. *The Dispersion and Structure of the Field Near L1688*

As illustrated in Figure 6, there is not much of a pattern to the mapped line-of-sight field strength within the L1688 region. Instead, the variation in the masured field strength arises from anisotropy in the field, which is due to actual field bending (with respect to the line of sight), or variations in total field strength, or both. Figure 7 shows the distribution of $B_\parallel$ for the self-absorption detections in Table 1 with $\alpha_{1950} < 16^h26^m$ (encompassing the region we refer to as "near L1688"). A Gaussian fit to the distribution in Figure 7 is centered at $B_{0_z} = 8.7$ μG, and has a 1 σ dispersion of 3.4 μG. A small part of the dispersion is due to the uncertainty (typically ~ 1.7 μG) in each measurement. In order to estimate the true dispersion in the field distribution, the measurement uncertainty needs to be subtracted in quadrature. After this subtraction, we find a "corrected" dispersion in the line-of-sight field, $\sigma_{B_z} = 2.9$ μG. (Note that in this section the subscript z refers to the line-of-sight properties of $\boldsymbol{B}$. The subscript x will be used below when referring to the plane-of-the-sky component of $\boldsymbol{B}$.)

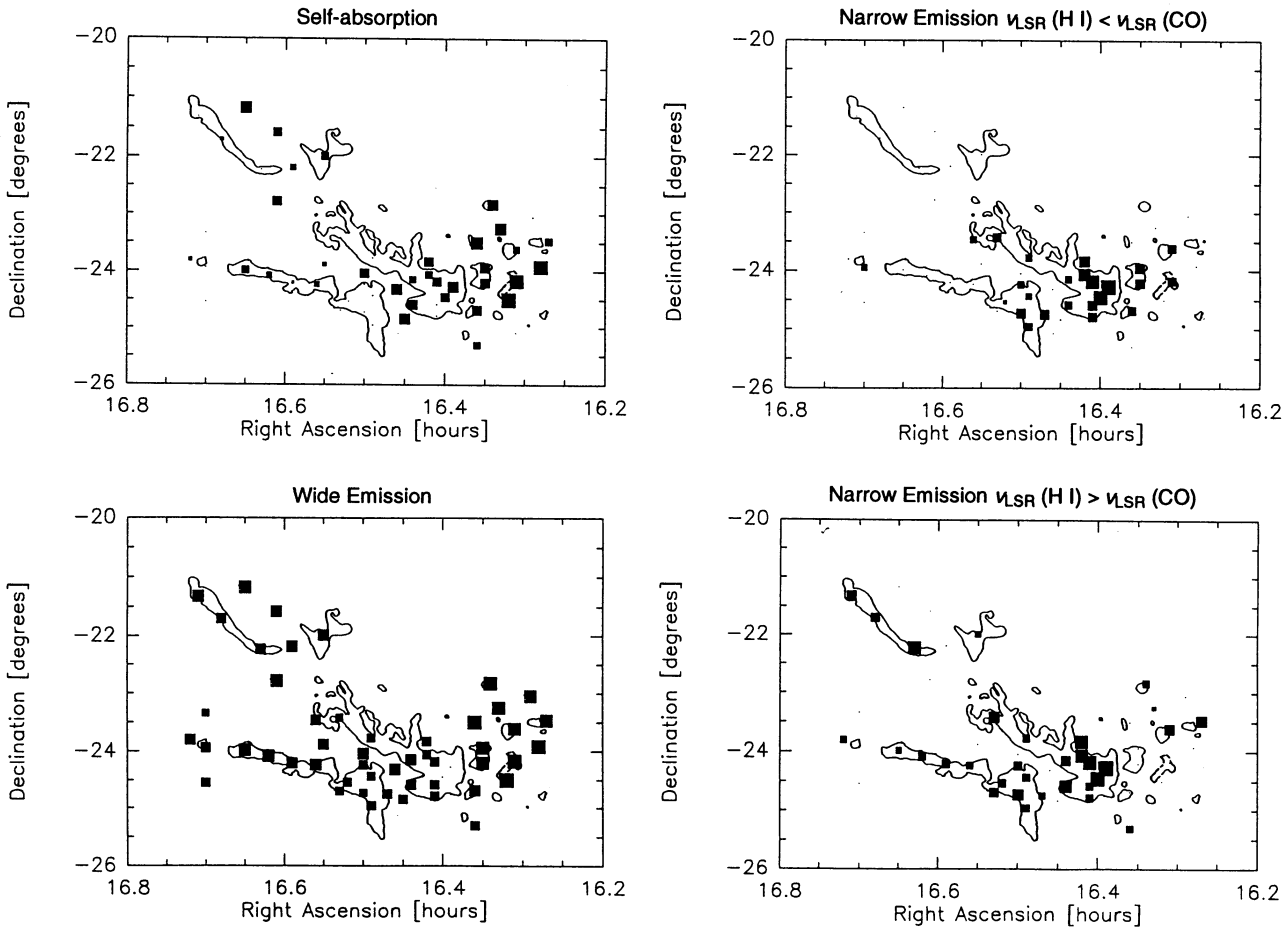

FIG. 5.—Spatial distribution of the self-absorption, narrow emission, and wide emission components fit to the H I spectra listed in Table 1, superposed on a contour map of molecular emission. The narrow emission components where $v_{DIFF} > 0$ and where $v_{DIFF} < 0$ are shown separately. The linear size of the filled square at each position is proportional to the strength the component at the position of that square. The solid contour is the $T_R^* = 3$ K contour of ^{13}CO, and the dashed contour near the western end of the map is a $T_R^* = 1$ K contour of ^{13}CO, from Loren (1989a).

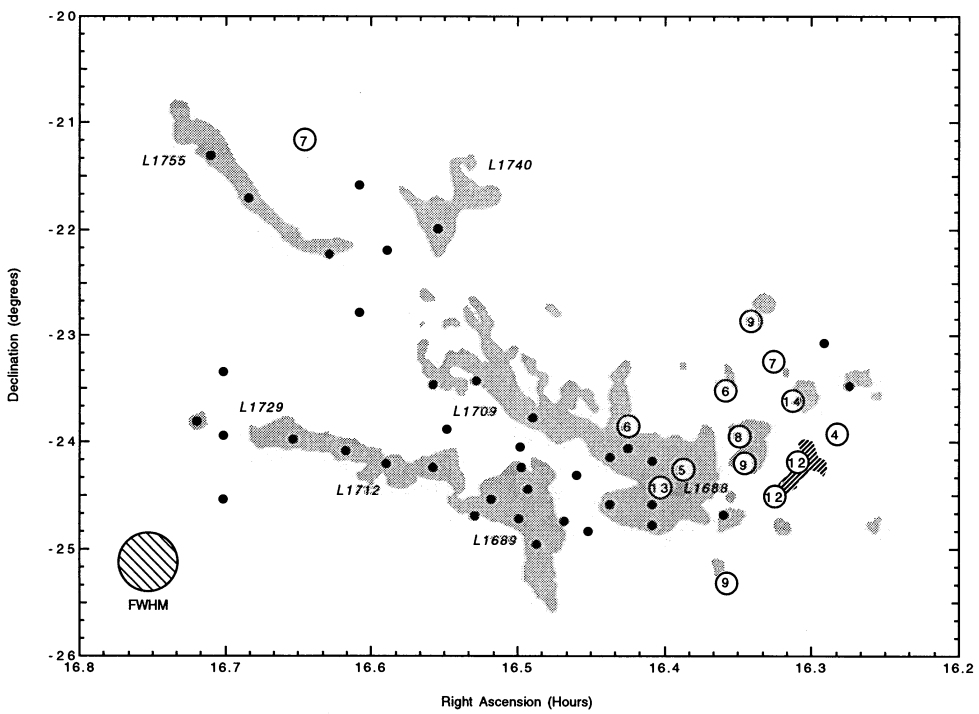

FIG. 6.—Magnetic field measured in H I self-absorption in Ophiuchus. Numbers in circles represent the field, in μG, fit to the self-absorption component of the spectra in Table 1. Black dots show positions surveyed where no significant field in a self-absorption component was detected. Shaded areas represent the molecular clouds in the Ophiuchus complex, with the area enclosed by the $T_R^* = 3$ K contour filled in gray and the less intense emission ($T_R^* = 1$ K contour) filled with stripes (Loren 1989a). The FWHM of the Hat Creek beam is also shown.

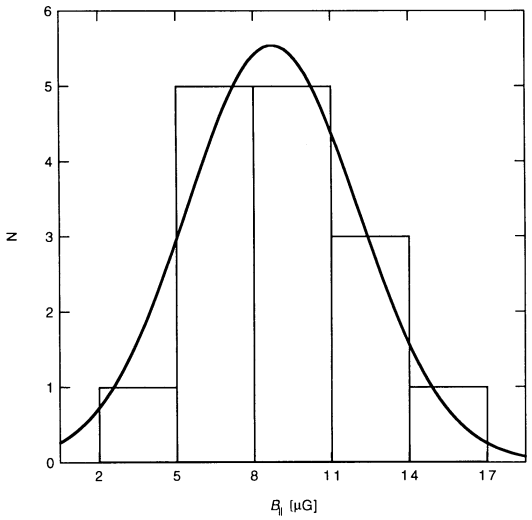

FIG. 7.—Distribution $B_{\|}$ near L1688. The histogram shows the values of $B_{\|}$ for the self-absorption detections in Table 1 with $\alpha_{1950} < 16^h26^m$. The solid line represents a least-squares Gaussian fit to the distribution.

The high degree of anisotropy in the line-of-sight magnetic field implied by the Zeeman observations is also seen in the plane-of-the-sky field structure near L1688. Both optical (Vrba et al. 1976, hereafter VSS) and near-infrared (Wilking et al. 1979) polarization observations show that the dispersion in polarization position angle is unusually high in this region, compared to the surrounding area. Myers & Goodman (1991, hereafter MG91) have suggested that the dispersion in the field is high due to the fact that gravitational forces overpower magnetic ones in regions forming clusters of stars, like L1688. Shocks present in the region, created by the interaction of the expanding wind discussed in § 3.1 with the dense gas in L1688, are also likely to bend field lines, on both large and small scales.

Figure 8 shows a composite view of magnetic fields for the L1688 region. Optical polarimetry traces the structure of the field projected onto the plane of the sky (VSS), and the strength and variation of the line-of-sight field is given by the Zeeman observations. If we can show that these independent data sets sample the same region along the line of sight, then we can combine the polarimetry and Zeeman observations into a three-dimensional picture of the field, as MG91 did for the dark cloud L204.

In Ophiuchus, self-absorption in H I occurs only along lines of sight where $A_V > 1$ mag (Minn 1981). Optical polarimetry traces out the plane-of-the-sky projection of whatever field has aligned grains along the line of sight to background stars seen through regions with average extinction of *less than about 2 magnitudes*. Along particular lines of sight, however, optical polarimetry can apparently sample higher extinction regions. In Ophiuchus, VSS claim that their optical observations sample primarily lines of sight with $1 < A_V < 10$ mag. So, it is possible that the same field is sampled by H I absorption Zeeman measurements and optical polarimetry. Infrared polarimetry should be able to penetrate even denser regions. Wilking et al. (1979) observed the linear polarization of background starlight in the L1688 region at 2.2 μm, through as much as 30 magnitudes of extinction, in a 24′ × 36′ area near the core of L1688. The mean field direction (22° ± 11°) and dispersion (34° ± 10°) implied by the Wilking et al. infrared polarimetry are very similar to the direction (32° ± 7°) and dispersion (31° ± 6°) implied by the VSS optical polarimetry for the region shown in Figure 8. Thus, it is possible that the optical and infrared polarimetry are tracing fields in similar regions. In light of all of this, we conclude that it is likely that the optical polarimetry and the self-absorption Zeeman observations shown in Figure 8 *are* both illustrative of the field in the region along the line of sight near the dark molecular clouds in L1688.

In order to combine the Zeeman data with the polarization data in Figure 8, we use a technique for describing field nonuniformity outlined by MG91 (see also Chandrasekhar & Fermi 1953; Jones 1989; Zweibel 1990; Jones, Klebe, & Dickey 1992). The ratio of uniform to nonuniform field is estimated from fits to the distribution of polarization position angle (θ_E) where the only free parameters are the mean position angle, $\bar{\theta}_E$, and

$$s = \frac{\sigma_B}{N^{1/2} B_{0x}}, \tag{2}$$

where σ_B is the width of a Gaussian-random distribution characterizing the nonuniform field (a.k.a. the typical strength of the nonuniform field), N represents the number of field decorrelation lengths along the line of sight, and B_{0x} represents the strength of the uniform field in the plane of the sky. For cases where the distribution of θ_E is centrally peaked and is well fitted by a Gaussian, s is equal to the 1 σ dispersion of the Gaussian, in radians. The parameter s is representative of the ratio of nonuniform to uniform field strength, in cases where N is comparable. In general, small values of s imply a highly ordered field and/or a large number of correlation lengths. Larger values of s often imply greater disorder in field structure, since N is restricted to be no less than one.

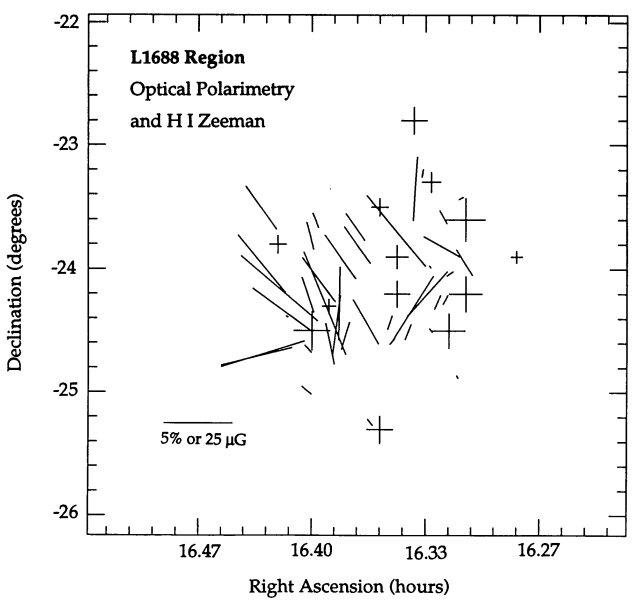

FIG. 8.—"Three-dimensional" field in L1688. Optical polarization vectors whose lengths are proportional to p(%) and whose orientations give θ_E (Vrba et al. 1976) map out the structure of the plane-of-the-sky field. Crosses, with size proportional to $B_{\|}$ as determined via detection of the Zeeman effect in H I self-absorption at the positions of the crosses, show the spatial variation in the line-of-sight field.

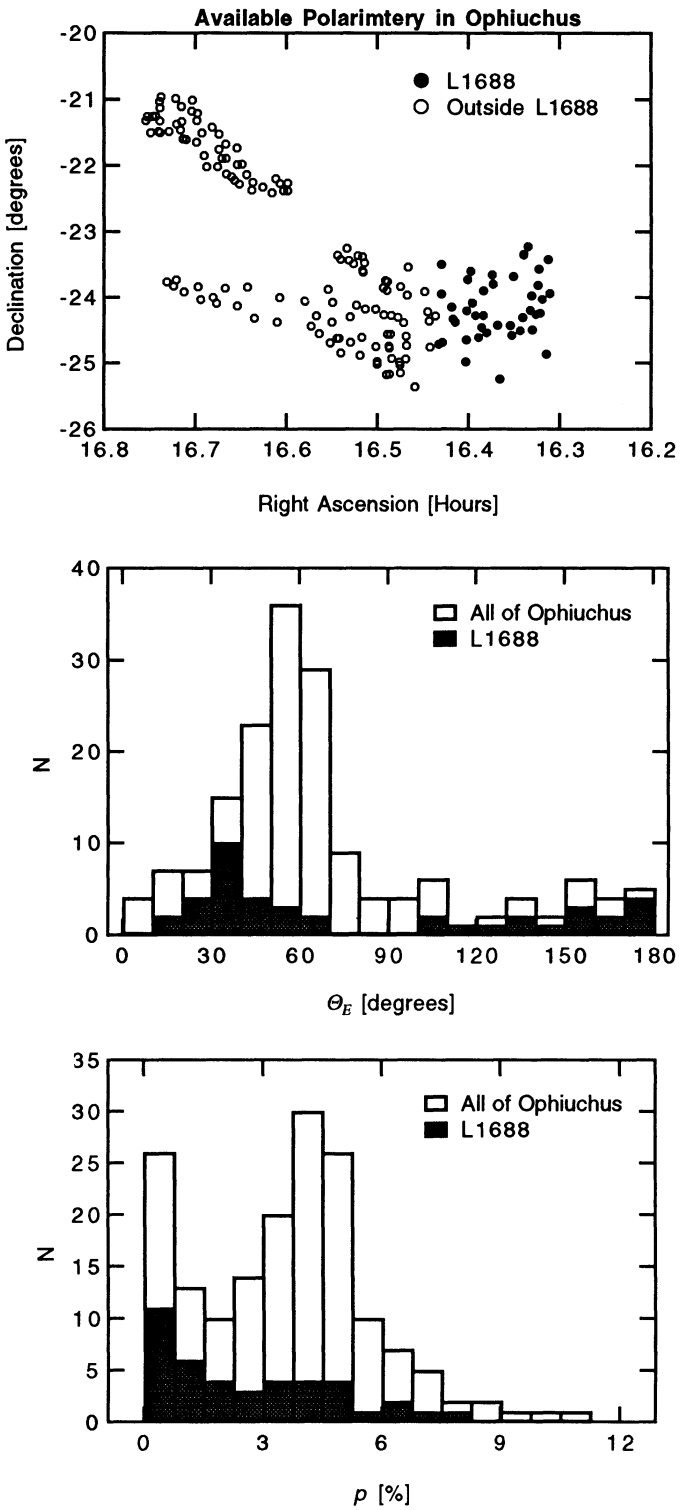

FIG. 9.—Distribution of percentage polarization for the L1688 region, as contrasted with all of Ophiuchus. The dots in the top panel show the positions of all the stars for which optical polarimetry is available (Vrba et al. 1976; Goodman et al. 1990), and the darker dots correspond to data points in the region with $\alpha_{1950} < 16^h26^m$, which we call "near L1688." These points are shown in shaded histograms in the lower two panels. The middle panel shows that the mean position angle of polarization in L1688 is different from the rest of the Ophiuchus complex, and the lower panel shows that the percentage polarization is typically much smaller in L1688 than elsewhere in the complex.

For the region shown in Figure 8, using the optical polarimetry in VSS (shaded points in Fig. 9), we find $s = 0.54 \pm 0.11$, which, as mentioned above, is significantly larger than the value, $s = 0.34 \pm 0.03$, derived from a fit to the data covering the entire Ophiuchus complex (MG91). The middle panel of Figure 9 shows the distributions of θ_E from which these two values of s are derived. The relatively large value of s associated with the L1688 region implies either a decrease in N relative to the surrounding area, which seems unlikely, or an increase in the proportion of nonuniform to uniform field (see eq. [2]).

An increase in field nonuniformity will tend to decrease the percentage of linear polarization observed in observations of background starlight (Jones 1989; Jones et al. 1992). Figure 9 shows the distribution of p, the percentage of linear polarization, in the vicinity of L1688, in comparison with the overall distribution for Ophiuchus. It is clear that the percentage polarization in this dense region is substantially lower than in its environs, implying a dramatic decrease in the ratio of polarization-to-extinction, p/A_V, in region near L1688. VSS note this decrease and conclude that grain alignment decreases rapidly in this region. Carrasco, Strom, & Strom (1973) conclude that the typical grain size in the dense regions of Ophiuchus is anomalously large. Decreases in p/A_V can be caused by field tangling (i.e., "an increase in field nonuniformity"), poor grain alignment in even an untangled field, depletion onto grains which creates larger, rounder grains, a change in grain composition which causes low polarization efficiency, *or* some combination of these effects. Sorting these possibilities out is difficult (Goodman et al. 1992, 1994), but given the significant increase in s in L1688 compared with its surroundings, we suspect that field tangling contributes substantially to the decrease in p/A_V.

Using the mean (B_{0z}) and dispersion (σ_{Bz}) in the line-of-sight field ($B_\parallel$) from the Zeeman observations, and the value of s from the fit to the optical polarization data, we can use the results of MG91 to describe the magnetic field near L1688 in three dimensions. Table 2 summarizes the properties of the field for a range of values of N, for a wavelike (Gaussian-random in two dimensions) and a turbulent (random in three dimensions) nonuniform field. In the turbulent case, we find that the angle i between $\boldsymbol{B}_0$ and the line of sight is 32°, the mean plane-of-the-sky field, B_{0x}, is 5.4 μG; and the total uniform field,

$$B_0 = |\boldsymbol{B}_0| = \sqrt{B_{0z}^2 + B_{0x}^2}\,, \tag{3}$$

is 10.2 μG. Thus, for the case where the nonuniform field is random in three dimensions, we can express the three-dimensional uniform field, according to MG91 (eq. [35]) as

$$\boldsymbol{B}_0 = 10.2\ \mu\text{G}\ [\pm(0.85\hat{N} + 0.53\hat{E}) + 0.85\hat{z}]\,, \tag{4}$$

where $\hat{N}$ and $\hat{E}$ represent unit vectors pointing north and east on the sky, and $\hat{z}$ is the unit line-of-sight vector. (Note that a twofold ambiguity in the direction of $\boldsymbol{B}$ always remains, because polarimetry can only give the direction of the plane-of-the-sky field modulo 180°.)

The nonuniform field is characterized by σ_B. Table 2 shows that σ_B ranges from about 3 to 9 μG in the turbulent case, depending on the choice of N. The total (uniform + nonuniform) field,

$$\langle B^2\rangle^{1/2} = (B_0^2 + D\sigma_B^2)^{1/2}\,, \tag{5}$$

is 14.3 μG, for the case where $N = 4$ and D, the number of

TABLE 2

THE MAGNETIC FIELD NEAR L1688 IN THREE DIMENSIONS

D	N	B_{0z} (μG)	σ_{B_z} (μG)	s	i	B_{0x} (μG)	B_0 (μG)	σ_B (μG)	$\langle B^2\rangle^{1/2}$ (μG)	M_n/M_u
3.....	1	8.7	2.9	0.54	32°	5.4	10.2	2.9	11.4	0.2
	4	8.7	2.9	0.54	32	5.4	10.2	5.8	14.3	1.0
	9	8.7	2.9	0.54	32	5.4	10.2	8.7	18.2	2.2
2.....	1	8.7	2.9	0.54	42	8.0	11.8	4.3	13.3	0.3
	4	8.7	2.9	0.54	42	8.0	11.8	8.6	16.9	1.1
	9	8.7	2.9	0.54	42	8.0	11.8	12.9	21.7	2.4

NOTES.—The column headings correspond to the variables used to describe the three-dimensional field in the text of this paper, and in MG91. The calculation is done for three values of the number of field correlation lengths, N, and for the case "$D = 3$," where the nonuniform field is random in three dimensions (turbulent), and "$D = 2$," where the nonuniform field is random in two dimensions (wavelike).

dimensions in the nonuniform component, is 3. The ratio of energy in the nonuniform field (M_n) to energy in the uniform field (M_u) is

$$\frac{M_n}{M_u} = \frac{D\sigma_B^2}{B_0^2}, \tag{6}$$

which is approximately unity for values of $N \approx 4$, a result which agrees well with the models of Jones et al. (1992).

The values for i, B_{0x}, B_0, σ_B, $\langle B^2\rangle^{1/2}$, and M_n/M_u depend on the value of D, and they are tabulated in Table 2 for the $D = 2$ wavelike case, as well as for the $D = 3$ case discussed above. In both cases, we find that the nonuniform and uniform field would contribute equal energy in the L1688 region if the number of correlation lengths of the field is of order 4.

4. DISCUSSION

4.1. *The Role of the Magnetic Field in Ophiuchus*

Ideally, we would like to associate each of our magnetic field strength measurements with a particular piece of the Ophiuchus dark cloud complex. It is very difficult to do this, for several reasons. Since the interstellar medium (ISM) is predominantly neutral atomic hydrogen, picking out a particular "clump" of gas from H I spectral line maps made with a large beam is a great challenge. We have established, based on an analysis of LSR velocities, that the self-absorption we see in the Ophiuchus H I spectra is likely to be associated with dense gas along the line-of-sight (§ 3.1). We cannot, however, *identify* particular molecular (e.g., ^{13}CO) clumps using only our H I observations. The H I beam is usually filled with much more gas than just that associated with a ^{13}CO clump along the line of sight. Therefore, it is not possible to compare field strengths predicted by physical models which require knowledge of clump mass, size, and velocity dispersion wth the measured field strengths on a clump-by-clump basis.

We cannot directly address issues such as whether a particular clump identified by Loren (1989a), in his ^{13}CO data, has more than, less than, or just enough magnetic energy to support itself against its own self-gravity. To do this, we would need field strength observations made in a tracer (e.g., OH) where the "clump" under study can also be identified in spectral line maps (Goodman et al. 1989). One should not use the H I Zeeman data in this paper to determine whether particular clumps of *molecular* gas are or are not magnetically supported. In order for Loren's clumps to be supported against gravity, he estimates that field strengths between about 10 and 300 μG are necessary—in the molecular gas (Loren 1989b). We find fields of order 10 μG in the atomic gas which is most likely to be associated with some of the lower density molecular gas, but we cannot comment on fields *within Loren's clumps.*

We can, however, take a more global view of the Ophiuchus Complex and use the H I data alone to learn about the role of the magnetic field on a scale larger than individual ^{13}CO clumps. If magnetic fields limit the magnitude of velocity fluctuations in the ISM, through wave motions, then the speed of an Alfvén wave, v_A, can be considered analogous to the sound speed in a gas where thermal motions dominate and temperature controls velocity dispersion. One can define an "Alfvén Mach number,"

$$m_A = \frac{\sigma\sqrt{3}}{v_A}, \tag{7}$$

where σ represents velocity dispersion, which is related to FWHM line width, Δv, by the expression $\sigma = \Delta v/(8\ln 2)^{1/2}$. When kinetic and magnetic energy are in rough equipartition, $m_A \sim 1$ (Bertoldi & McKee 1992; Myers & Goodman 1988).

The Alfvén speed depends only on magnetic field strength, B, and gas density, ρ,

$$v_A = \frac{B}{\sqrt{4\pi\rho}}. \tag{8}$$

So, if ρ is known at the position of each Zeeman observation, and B can be estimated from $B_{\|}$, then line width and Alfvén speed can be compared in the context of the Alfvén Mach number. At the positions where the H I Zeeman effect has been detected in self-absorption in Ophiuchus, we have enough information to approximate v_A. We cannot directly determine the volume density of H I along each line of sight without knowing the background temperature and line-of-sight gas distribution. But, we can estimate an average density for these positions, by using the argument that one needs $A_v > 1$ mag to see H I in self-absorption (see § 3.4). If we assume that the line-of-sight extent of the L1688 region is approximately the same as its extent on the sky (1°.2 = 2.6 pc at 125 pc distance), then a column density of H I of $N = 3.3 \times 10^{20}$ cm^{-2}, corresponding to $A_V = 1$ mag (de Geus & Burton 1991) gives a particle density $n = 40$ cm^{-3}. Note that we have chosen to use the $N/A_V = 3.3 \times 10^{20}$ cm^{-2} mag^{-1} ratio derived by de Geus & Burton (1991) which is based on *IRAS*, H I, and extinction measurements in Ophiuchus, rather than the average value for the ISM, $N/A_V = 1.9 \times 10^{21}$ cm^{-2} mag^{-1} (Bohlin, Savage, & Drake 1978). In reality, the regions producing self-absorption are smaller than the whole of the L1688 region, and their

individual extinctions higher, but we cannot be off in our density estimate by too much since densities much higher than 40 cm^{-3} will lead to formation of too much H_2 to see much H I and lower densities are not likely to produce self-absorption in Ophiuchus.

Figure 10 presents a comparison of v_A (calculated for $n = 40$ cm^{-3}) and the line width, at each of the positions where the H I Zeeman effect is detected in self-absorption. The figure assumes $B = B_{||}$, which is not true when the field is not along the line of sight. In § 3.4 we found that the angle between the line of sight and the average field, B_0, is about 32° in the L1688 region, which implies $B_0/B_{0z} = 1.2$. But, given the large uncertainty associated with estimating the density (~a factor of 2) used to calculate v_A in Figure 10, we have chosen not to apply this small correction factor to the field, which would increase v_A by a factor of 1.2. Amazingly enough, even with all of these assumptions, *the distribution of Alfvén speeds and the distribution of line widths in the L1688 region are remarkably similar* (bottom two panels of Fig. 10). No detailed correlation between v_A and Δv is evident (top panel), but this is almost to be expected, given that a single density was assumed for all points, and the inclination angle of the field is not known at each point. Keep in mind that a change of a factor of 4 in density will change v_A by a factor of 2, which moves an individual point across most of the range of v_A spanned in Figure 10.

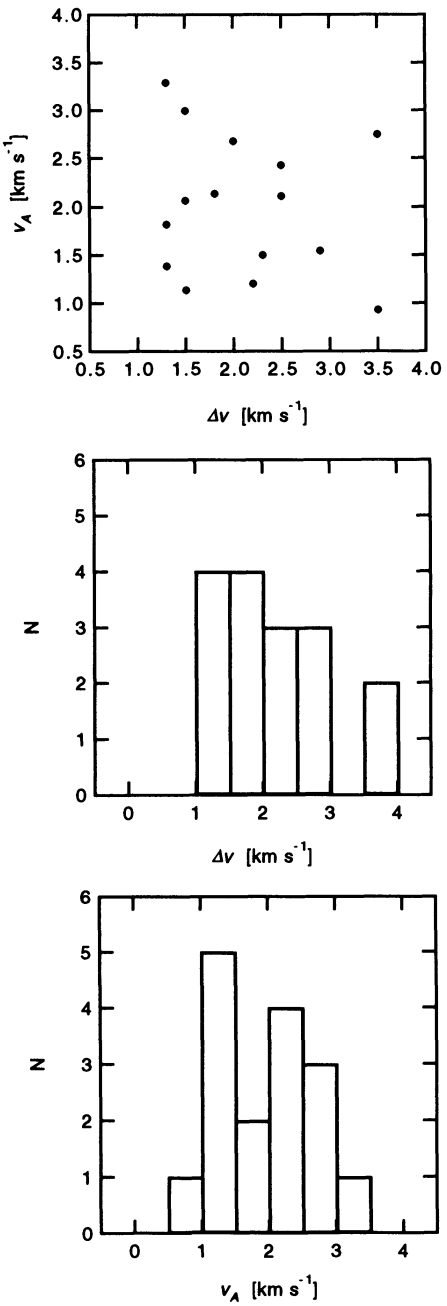

FIG. 10.—Alfvén speed as a function of line width for the fields measured via detection of the H I Zeeman effect in self-absorption. Here n is assumed to be 40 cm^{-3}. The lower two panels show that the overall distributions of line width and Alfvén speed are very similar, despite poor agreement on a point-to-point basis (*top panel*).

The average values of v_A and Δv are 2.0 and 2.1 km s^{-1}, respectively, for the data in Figure 10. Therefore, equation (7) gives $m_A = 0.8$ as an average value for the region of Ophiuchus where self-absorption is observed in H I. For $m_A = 1$, which represents equipartition of magnetic and kinetic energy, the average density would need to be 66 cm^{-3} if we assume $B = B_{||}$, or 95 cm^{-3} for $B = 1.2B_{||}$. For $m_A \gg 1$, MHD turbulence becomes highly dissipative. Bertoldi & McKee (1992), in their model of "pressure-confined clumps in magnetized molecular clouds," conclude that m_A does not depend on clump mass and can be considered characteristic of a particular system of clumps (e.g., a complex). So, we can compare their estimate of m_A, which is based on ^{13}CO data, with ours. In Ophiuchus, using an assumed field of 20 μG, they estimate m_A to be 0.75 for prolate (2 : 1 aspect ratio), pressure-confined, non–self-gravitating clumps, or 1.2 for spherical clumps. These theoretical estimates of m_A, which used an assumed field strength, and ^{13}CO-derived clump parameters, are in very good agreement with our estimate of $m_A = 0.8$.

5. SUMMARY

We have measured the strength of the magnetic field in the atomic gas associated with the Ophiuchus Dark Cloud complex, via detection of the Zeeman effect in the 21 cm lines of atomic hydrogen. In order to extract the field strengths, we decomposed the spectral line profiles into three or four components at each position, only one or two of which have LSR velocity near that of the molecular gas in Ophiuchus. In cases where a self-absorption component is present in the spectrum, its velocity usually agrees most closely with the molecular gas velocity, and we take the field strengths measured in self-absorption to be most representative of the dark cloud complex. Almost all of the self-absorption detected in Ophiuchus is associated with the region near the star-forming dense cloud L1688.

For the region near L1688, using the VSS optical polarization data to describe the plane-of-the-sky field, and our H I Zeeman results to describe the line-of-sight field, we estimate the strength, direction, and uniformity of the three-dimensional magnetic field in the context of the MG91 model. The mean uniform field derived from the model is 10.2 μG, inclined to the line of sight by 32°. In a case where the nonuniform field is isotropic in three dimensions, and the field has four correlation lengths along the line of sight, the typical strength of the nonuniform field is ~6 μG, and the ratio of energy in the uniform and nonuniform fields is about one. Table 2 presents model

predictions for the nature of the field under several other sets of conditions.

If the average density in the self-absorption producing gas is 40 cm^{-3}, then the Alfvén Mach number near L1688 is of order unity, and magnetic and kinetic energy are roughly equal.

We are grateful to Frank Bertoldi, Eugène de Geus, Chris McKee, and Phil Myers for insightful comments on this work. Carl Heiles thanks the NSF for support through grant AST-91-23362.

REFERENCES

Bertiau, F. C. 1958, ApJ, 128, 533
Bertoldi, F., & McKee, C. F. 1992, ApJ, 395, 140
Blaauw, A. 1964, ARA&A, 2, 213
Bohlin, R. C., Savage, B. D., & Drake, J. F. 1978, ApJ, 224, 132
Cappa de Nicolau, C. E., & Pöppel, W. G. L. 1986, A&A, 164, 274
Carrasco, L., Strom, S. E., & Strom, K. M. 1973, ApJ, 182, 95
Chandrasekhar, S., & Fermi, E. 1953, ApJ, 118, 116
Crutcher, R. M., Troland, T. H., Goodman, A. A., Kazès, I., Heiles, C., & Myers, P. C. 1993, ApJ, 407, 175
de Geus, E. J. 1988, Ph.D. thesis, Sterrewacht Leiden
———. 1992, A&A, 262, 258
de Geus, E. J., Bronfman, L., & Thaddeus, P. 1990, A&A, 231, 137
de Geus, E. J., & Burton, W. B. 1991, A&A, 246, 559
de Geus, E. J., de Zeeuw, P. T., & Lub, J. 1989, A&A, 216, 44
Evans, N. J., II, & Lada, E. A. 1991, in Fragmentation of Molecular Clouds and Star Formation, ed. E. Falgarone & G. Duvert (Dordrecht: Kluwer), 293
Goodman, A. A. 1989, Ph.D. thesis, Harvard University
Goodman, A. A., Bastien, P., Myers, P. C., & Ménard, F. 1990, ApJ, 359, 363
Goodman, A. A., Crutcher, R. M., Heiles, C., Myers, P. C., & Troland, T. H. 1989, ApJ, 338, L61
Goodman, A. A., Jones, T. J., Lada, E. A., & Myers, P. C. 1992, ApJ, 399, 108
Goodman, A. A., Jones, J. J., Lada, E. A., & Myers, P. C. 1994, in preparation
Heiles, C. 1988, ApJ, 324, 321
Heiles, C., & Stevens, M. 1986, ApJ, 301, 331
Jones, T. J. 1989, ApJ, 346, 728
Jones, T. J., Klebe, D., & Dickey, J. M. 1992, ApJ, 389, 602
Loren, R. B. 1989a, ApJ, 338, 902
———. 1989b, ApJ, 338, 925
Loren, R. B., Wooten, A., & Wilking, B. A. 1990, ApJ, 365, 269
Minn, Y. K. 1981, A&A, 103, 269
Mundy, L. G., Wooten, H. A., & Wilking, B. A. 1990, ApJ, 352, 159
Myers, P. C., & Goodman, A. A. 1988, ApJ, 329, 392
———. 1991, ApJ, 373, 509 (MG91)
Myers, P. C., & Ho, P. T. P. 1975, ApJ, 202, L25
Myers, P. C., Ho, P. T. P., Schneps, M. H., Chin, G., Pankonin, V., & Winnberg, A. 1978, ApJ, 220, 864
Nozawa, S., Mizuno, A., Teshima, Y., Ogawa, H., & Fukui, Y. 1991, ApJS, 382, 361
Ross, F. E., & Calvert, M. R. 1934, Atlas of the Northern Milky Way (Chicago: Univ. Chicago Press)
Sancisi R., & van Woerden, H. 1970, A&A, 5, 135
Sato, S., et al. 1988, MNRAS, 230, 321
Tamura, M., Hayashi, S., Yamashita, T., Duncan, W. D., & Hough, J. H. 1993, ApJ, 404, L21
Tamura, M., Sato, S., Suzuki, H., Kaifu, N., & Hough, J. 1990, ApJ, 350, 728
Troland, T. H., & Heiles, C. 1982, ApJ, 252, 179
Vrba, F. J., Strom, S. E., & Strom, K. M. 1976, AJ, 81, 958 (VSS)
Wilking, B. A. 1992, in Low Mass Star Formation in Southern Molecular Clouds, ed. B. Reipurth (ESO Scientific Rept. 11), 159
Wilking, B. A., & Lada, C. J. 1983, ApJ, 274, 698
Wilking, B. A., Lebofsky, M. J., Rieke, G. H., & Kemp, J. C. 1979, AJ, 84, 199
Zweibel, E. G. 1990, ApJ, 362, 545